Ultrasensitive frequency-modulation spectroscopy enhanced by a high-finesse optical cavity: theory and application to overtone transitions of C_2H_2 and C_2HD

Long-Sheng Ma,* Jun Ye, Pierre Dubé,† and John L. Hall‡

JILA, University of Colorado and National Institute of Standards and Technology, Boulder, Colorado 80309-0440

Received February 17, 1999; revised manuscript received June 8, 1999

The sensitivity of FM spectroscopy can be dramatically enhanced by location of the sample in a high-finesse cavity, for example, ~5 orders of magnitude in this study. To avoid conversion of laser frequency noise into amplitude noise by the cavity, we choose the rf modulation frequency to match the cavity's free spectral range. In this way small frequency fluctuations produce no additional noise, and a pure FM dispersion signal is recovered in transmission. We present a systematic study of the detection sensitivity, signal line shape and size, and slope at the central tuning. Experimentally, using a weakly absorbing gas such as C_2H_2 or C_2HD placed inside an external high-finesse resonator, we obtained an integrated absorption sensitivity of 5×10^{-13} (1×10^{-14}/cm) for the gas's weak near-IR molecular overtone transitions. As an interesting application, a Nd:YAG laser was well stabilized on the $P(5)$ line of the C_2HD ($\nu_2 + 3\nu_3$) band by this technique. The high attainable sensitivity permitted selection of slow molecules with low power and gas pressure to give a linewidth 13 times below the room-temperature transit-time limit. [S0740-3224(99)01711-7]

OCIS codes: 300.6380, 300.6360, 300.6340.

1. INTRODUCTION

The invention of frequency-modulation (FM) laser spectroscopy in the 1980's has brought us a shot-noise-limited absorption detection sensitivity of 10^{-7}.[1] This rf technique has also been used widely and successfully in optical frequency metrology, for example, in stabilizing lasers to sub-Hertz linewidths[2] in short-term and to 300 Hz in long-term reproducibilities.[3] The increasing need for high-quality optical frequency standards in the visible and the near IR has stimulated a number of recent high-precision studies of molecular overtone transitions.[4,5] Molecular overtones can provide many comblike resonances that cover a broad spectrum in the visible and near-IR regions, whereas the linewidths potentially are in the subkilohertz domain that is characteristic of the decay rates of fundamental molecular stretch resonances. The absence of a fast decay route results in higher values of the resonance Q and so should provide more stable and reproducible locking onto the resonance line center. Hence one can hope with a simple gas, such as acetylene (C_2H_2), to build a highly interlinkable network of optical frequency standards with excellent frequency stability and reproducibility.

However, overtone transitions arise from the anharmonicity of molecular vibrations and are usually quite weak. For example, the fourth or fifth order of overtone is needed to reach the visible domain, and the oscillator strength would correspondingly decrease by a factor of $\sim 10^6$ compared with that of the fundamental. This extremely low level of absorption presents a sensitivity challenge to any direct absorption spectroscopic method, even when one is using the FM approach. Furthermore, we would also need a high intensity of light to obtain an appropriate level of saturation to provide access to nonlinear sub-Doppler resonances. Therefore one could say that the major difficulty to be overcome in achieving a grid of molecular overtone–based optical frequency standards is the need to find a simple method to saturate these lines and detect them with sufficiently high signal-to-noise ratios (S/N's). Following earlier research by Cerez *et al.*[6] demonstrated the possibility of improving the detection sensitivity by placing their I_2 absorption cell in an external optical cavity (working with a He–Ne laser at 612 nm). Subsequently, we combined the FM technique and low-finesse external cavities to improve the I_2 saturation signals at 612 nm (Ref. 7) and more recently also used cavity enhancement to observe some very weak higher-order overtone lines, namely, the $\nu_1 + 3\nu_3$ band of C_2H_2 at 790 nm,[5] in the near visible. To our knowledge, the intracavity method to observe saturated absorption spectra of molecular overtone lines was first applied by de Labachelerie *et al.*,[4] and, indeed, they obtained spectacular saturated absorption resonances in the $\nu_1 + \nu_3$ band of C_2H_2 at 1.55 μm. As will be discussed momentarily, we recently learned how to work without increased noise by using optical cavities of very high finesse ($\sim 10^5$). In this way we extended this cavity-enhancement strategy to increase the S/N of a high overtone transition of C_2H_2 at 790.7 nm (Ref. 8) and to observe and study the even weaker $P(5)$ line of mono-deuterated acetylene [$C_2HD(\nu_1 + 3\nu_3)$] at 1064 nm.[9,10]

In this paper we begin with a detailed discussion of the principles of the new method. We then describe the experimental setup that has led us into the $\sim 10^{-13}$ domain

0740-3224/99/122255-14$15.00

of an integrated absorption sensitivity and discuss one application of the method: to precisely lock a diode-laser-pumped Nd:YAG laser (MISER) onto an overtone transition of C_2HD. An interesting benefit of the extreme sensitivity of the method is that it affords the possibility to observe linewidth narrowing by optically selecting slow molecules. In Section 5 below, we discuss the possibility of approaching a resolution of tens of kilohertz and a frequency stability of 10^{-14} at 1-s averaging time and of measuring weak linear absorption precisely by a method based on locking a stable, but slightly tunable, oscillator onto the cavity's free-spectral-range (FSR) modes.

2. PRINCIPLES

A. Absorption and Saturation Power for Overtone Transitions

Inasmuch as the dipole moments of molecular high-overtone transitions are in the domain of a few hundred micro-Debye (1 Debye = 3.33564×10^{-30} C m), the absorption is very weak at a pressure of a few millitorr (1 Torr = 133 Pa). For example, the linear absorption coefficient of the $P(11)$ line of the $\nu_1 + 3\nu_3$ band of C_2H_2 at 790.7 nm is $1.8 \times 10^{-5}\,\mathrm{cm^{-1}\,Torr^{-1}}$. For the $\nu_2 + 3\nu_3$ $P(5)$ line in C_2HD at 1064 nm it is $8.8 \times 10^{-7}\,\mathrm{cm^{-1}\,Torr^{-1}}$. For metrology purposes, we need to observe saturated absorption resonances to achieve the necessary narrow sub-Doppler linewidths. Such a saturated absorption feature may be, at best, tenfold smaller than the linear absorption for a realistic saturation parameter below 1. So the first consideration for the experimental setup is the sensitivity of detection.

Secondly, we wish to observe as narrow saturated absorption features as possible and so shall consider the saturation power at a lower pressure (~1 mTorr), where the collisional broadening is negligible compared with transit-time broadening $\Delta\nu_{\mathrm{FWHM}} = 2u_m/8w_0$ (in hertz).[11,12] [Here $u_m = (2K_BT/M)^{1/2}$ is the Maxwell velocity and w_0 is the laser mode radius.] We denote the half-width by $\Gamma_2 = 2\pi(u_m/8w_0)$. The condition for saturation becomes $\Omega_{\mathrm{Rabi}} = \mu E/\hbar = \Gamma_2$, which corresponds to a field $E_s = (\Gamma_2/\mu)\hbar = (u_m/8w_0)(2\pi/\mu)\hbar$. Here μ is the transition dipole moment. Because the molecules are located in a standing-wave cavity, the corresponding laser mode axial intensity in one direction is $(1/2)c\epsilon_0 E_s{}^2$ and the saturation power in one direction is therefore $P_s = (\pi/2)w_0{}^2(1/2)c\epsilon_0 E_s{}^2$. So we obtain $P_s = (\pi^3/64) \times (2K_BT/M)(\hbar^2 c\epsilon_0/\mu^2)$. For C_2H_2 at room temperature this coefficient corresponds to $0.24\mu W/\mu^2$, where μ is expressed in units of Debye. In Table 1 we list five C_2H_2- and C_2HD-related overtone transitions with their band positions and transition dipole moments. For the 1.06-μm band of C_2HD we see that the saturation power needed is ~51 W. We can also see that the saturation intensities for the higher-order overtone lines increase rapidly.

In practice, to maximize S/N the gas pressure is chosen to be ~10 mTorr, where the observed linewidth (including pressure broadening) is nearly twice the transit broadening. Consequently it requires four times more intensity to saturate this homogeneously broadened transition than the free-flight limit. Thus for these transitions we are led to consider cavities of high finesse, because high finesse also leads to large power buildup inside the cavity, giving saturation parameters close to 1 without requiring a large transmitted power to be accepted by the detector. Of course a high finesse will also greatly extend the overall effective molecular absorption length and thereby increase the resonance contrast in the cavity-transmitted light.

However, the fatal disadvantage of naïve use of a cavity with such high finesse is that the cavity naturally becomes an efficient laser-frequency discriminator, providing a huge conversion of residual laser-frequency noise into amplitude noise. Evidently high finesse exacerbates this conversion and leads to a catastrophic degradation of the achievable S/N performance relative to the theoretical shot-noise level.

Of course, we note that in practice one can readily achieve reasonably good laser locking onto the resonances of such cavities, even cavities of extremely high finesse. What is more difficult—perhaps not yet attained—is to achieve such precise locking that there is no degradation relative to the shot-noise-limited residual frequency variations.

We now discuss a new and powerful idea to capture the advantages of both FM detection and intracavity absorption enhancement while eliminating sensitivity to the laser/cavity relative frequency noise. We assume that the modulation sidebands for the FM detection are engineered to fall exactly on axial cavity resonances, shifted by one or more cavity FSR. Now when there are small frequency shifts of the laser and its sidebands about the exact cavity resonance frequencies, all these frequency components experience the same small phase shifts for their internal fields (unless a cavity mode resonance is shifted by molecular dispersion). Thus the transmitted beam remains purely FM despite small power fluctuation

Table 1. Strengths of C_2H_2 and C_2HD Vibration Overtone Bands at Five Selected Wavelengths

Molecule	Band Origin ($\mathrm{cm^{-1}}$)	Band Assignment	S_ν at 300 K ($\mathrm{cm^{-2}\,atm^{-1}}$)[a]	Studied Line Wavelength (nm)	Absorption ($\mathrm{cm^{-1}\,Torr^{-1}}$)	μ (mD)	P_{sat} (watts)	Ref.
$^{12}C_2H_2$	3288.58	ν_3	108.50(8)	3059.529, $P(11)$	0.81	42.98	1.3×10^{-4}	13
$^{13}C_2H_2$	6521.9	$\nu_1 + \nu_3$	1.1	1539.976, $P(12)$	3×10^{-3}	3.018	25×10^{-3}	14
C_2HD	9404.73	$\nu_2 + 3\nu_3$	0.00079	1064.470, $P(5)$	8.8×10^{-7}	0.069	49.6	15
$^{12}C_2H_2$	12675.7	$\nu_1 + 3\nu_3$	0.0102	790.703, $P(11)$	1.8×10^{-5}	0.212	5.4	16
$^{12}C_2H_2$	15600.2	$5\nu_3$	0.00154	642.233, $P(11)$	9.4×10^{-7}	0.076	42.5	17

[a] S_ν is the absolute band strength/intensity.

on the detector, and no unwanted detected noise results from small laser–cavity detunings at the modulation frequency. One could refer to this property of the new spectroscopic method as being frequency-noise immune.

FM spectroscopy has proved to be a successful method for avoiding excessive amplitude noise, whereby one performs modulation and detection of the signal in a frequency region where noise processes of whatever origin no longer possess strong power density. After a strong reduction of the Ti:sapphire laser frequency noise by improved frequency servo techniques, the use of this FM detection approach in an external cavity/gas cell system was clearly demonstrated.[5] With a superhigh-finesse cavity, however, the modulation frequencies become limited to the audio range, because sidebands of higher frequencies would lie outside the cavity resonance width and so would no longer be efficiently coupled into the cavity to probe the intracavity molecular resonance. In our new scheme, we frequency modulate the input laser beam at exactly $\Delta/2\pi = c/2L$, the FSR splitting frequency. Now we have the FM sidebands in a high-frequency region of low noise, and the cavity accepts the sidebands on resonance in exactly the same way as the carrier. The small frequency variations of the laser will still lead to some amplitude fluctuations and small optical phase shifts of the transmitted carrier as noted above, but they will also lead to exactly the same relative amplitude fluctuations and phase shifts of the sidebands, which are transmitted on adjacent (or nearby) axial orders. So the transmitted light still accurately represents a FM spectral triplet, with minimal amplitude modulation (AM) conversion that arises from the relative laser/cavity frequency jitter. Thus the noise level can approach the intrinsic AM noise level of the laser at the $c/2L$ FM detection frequency. Evidently, if the intracavity molecules are in resonance with the carrier or one of the sidebands they will weaken and phase shift this component, so there can be both absorption and dispersion components in the rf beat signal generated by the detector that is viewing the transmitted light. As the laser–cavity system is tuned over the molecular absorption, rf phase-sensitive demodulation will lead to the usual triplet spectrum of FM spectroscopy. We have given the acronym NICE-OHMS (noise-immune, cavity-enhanced optical heterodyne molecular spectroscopy) to this technique.

B. Cavity Enhancement

Figure 1 illustrates the conversion of incident power (P_{in}) into reflected (P_r), built-up (P_c), and transmitted (P_t) powers by the cavity. The cavity finesse F, (resonant) reflection R, transmission T, and enhancement E of light intensity by cavity buildup are described by the following formulas:

$$F = \frac{2\pi}{T_{\text{out}} + T_{\text{in}} + L_{\text{in}} + L_{\text{out}} + 2\alpha L}, \tag{1}$$

$$R = \frac{P_r}{P_{\text{in}}} = \left(\frac{T_{\text{out}} - T_{\text{in}} + L_{\text{in}} + L_{\text{out}} + 2\alpha L}{T_{\text{out}} + T_{\text{in}} + L_{\text{in}} + L_{\text{out}} + 2\alpha L}\right)^2, \tag{2}$$

$$T = \frac{P_t}{P_{\text{in}}} = \frac{4T_{\text{in}}T_{\text{out}}}{(T_{\text{out}} + T_{\text{in}} + L_{\text{in}} + L_{\text{out}} + 2\alpha L)^2}, \tag{3}$$

$$E = \frac{P_c}{P_{\text{in}}} = \frac{4T_{\text{in}}}{(T_{\text{out}} + T_{\text{in}} + L_{\text{in}} + L_{\text{out}} + 2\alpha L)^2}. \tag{4}$$

T_{in}, T_{out}, L_{in}, and L_{out} are the transmissions and losses of input and output coupling mirrors, respectively, α is the gas absorption per unit length, and L is the cavity length.

Assuming that $(2\alpha L)$ is much smaller than $(T_{\text{out}} + T_{\text{in}} + L_{\text{in}} + L_{\text{out}})$, we can derive from Eq. (3) that the use of a cavity of finesse F will increase the equivalent intracavity absorption length by a factor of

$$G = 2F/\pi. \tag{5}$$

We immediately see from Eqs. (1)–(5) that a high-finesse cavity increases the sensitivity to detect weak absorption. It also increases the light intensity, enabling us to reach the appropriate intensity for saturation. Therefore, as noted in Section 1, the molecular overtone transitions can be saturated and detected with a high SNR and with sub-Doppler resolution. Basically one is working at the shot-noise limit ($\leqslant 10^{-7}$) but with a contrast enhancement of G ($>10^4$).

C. Signal Line Shape

Our new technique is shown schematically in Fig. 2. Two separate optical frequency–phase modulations are applied to the laser beam by successive electro-optic modulators (EOM1 and EOM2). We use the modulation at low frequency $\delta/(2\pi)$ (a few megahertz) to obtain the cavity locking signal in the cavity-reflected beam. This cavity-reflected signal is of dispersion form and serves as the error signal for locking the laser onto a resonant mode of the high-finesse cavity. The modulation at high frequency $\Delta/(2\pi)$ (several hundred megahertz, matching the cavity FSR) is used to detect the weak saturated absorption of molecules contained inside the cavity by use of the cavity-transmitted beam.

Figure 3 illustrates the physical principle of the new technique, showing the way in which the molecular saturated dispersion causes an imbalance of the laser FM spectrum by means of a phase shift of the carrier component. Here ω_L denotes the laser frequency and Δ and δ are the phase-modulation frequencies generated by the high- and low-frequency EOM's, respectively. As we have already explained, modulation frequency Δ is chosen to match the FSR of the cavity, whereas δ is usually cho-

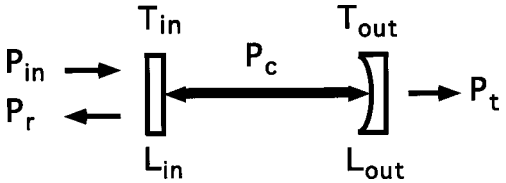

Fig. 1. Conversion of incident power into reflected, built-up, and transmitted powers. $T_{\text{in}}, T_{\text{out}}$ and $L_{\text{in}}, L_{\text{out}}$, transmissions and losses of input and output coupling mirrors, respectively. P_{in}, P_r, P_t, cavity input and reflected and transmitted light powers, respectively. P_c, one-way circulating light power.

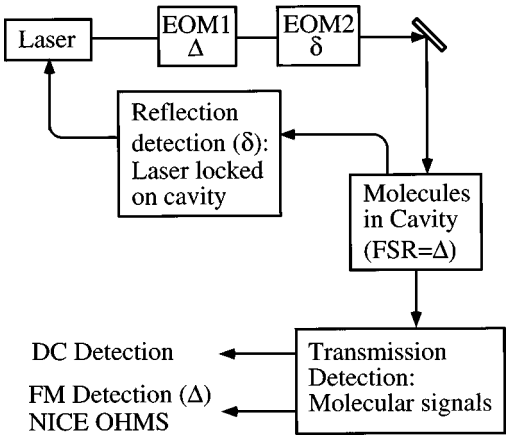

Fig. 2. NICE-OHMS detection scheme. Sidebands at δ are used for reflection lock to the cavity; sidebands at Δ, matching the cavity FSR, are used to probe the molecular saturated absorption in cavity transmission. Other abbreviations defined in text.

sen to be larger than the cavity linewidth. (The value $\delta/2$ fixes the Nyquist limit for the frequency-control loop bandwidth.) The laser spectrum now has three major components: the carrier at ω_L and two sidebands at $\omega_L \pm \Delta$. Additionally, each of them has its own two sidebands located at $\pm\delta$ away from itself, namely, at $\omega_L \pm \delta$, $\omega_L + \Delta \pm \delta$, and $\omega_L - \Delta \pm \delta$, as shown in Fig. 3(a). The beam reflected from the cavity carries all these frequency components and is detected by a P–I–N photodiode. Demodulation at frequency δ produces a servo error signal to lock the laser frequency onto the narrow-linewidth cavity. Because of the additional modulation, this locking error signal now has three contributions that additively define the lock point: two sideband resonances of strength $J_1(\beta)^2$ near $\omega_0 \pm \Delta$ and the carrier contribution $J_0(\beta)^2$ near ω_0, as shown in Fig. 3(b). (Here β is the FM index at Δ.) When none of the laser frequency components is affected by a resonance of the intracavity molecules, the servo error signal will simply keep the carrier ω_L and its two sidebands $\omega_L \pm \Delta$ at the cavity resonance centers ω_0 and $\omega_0 \pm$ FSR, respectively, as shown in Fig. 3(c). Thus the cavity transmitted beam has the original perfectly balanced FM spectra because the carrier ω_L and the sidebands $\omega_L \pm \Delta$ experience the same phase shifts and amplitude attenuations after they pass through the cavity. However, when a molecular resonance affects any of these three components, the additional interaction will certainly convert part of the FM into AM, which is then detected by a fast photodiode viewing the cavity-transmitted light. For example, as shown in Fig. 3(d), when the molecular resonance is present near the cavity resonance ω_0, the carrier will experience a modified intracavity refractive index that has been changed by Δn because of the molecular nonlinear saturated absorption. As a result, ω_0 is shifted by $\nu_m = -\omega_0 \Delta n$. If we neglect for the moment the servo contributions from the two sidebands, then the carrier ω_L can be kept at the new cavity resonance center ($\omega_0 + \nu_m$), and the sidebands, after being shifted to the new positions of $\omega_L \pm \Delta + \nu_m$, will no longer perfectly line up with the cavity resonances shown in Fig. 3(d). The resultant phase shifts then lead to the AM signal recovered by the transmission detector. [In practice, the two sidebands contribute certain servo error components that will partially offset the servo error signal provided by the carrier. The net result is that the laser frequency will be shifted back by the laser servo in the amount $x = 2\nu_m \times J_1(\beta)^2$, as shown in Fig. 3(e), where x is derived from the requirement that $xJ_0(\beta)^2 - 2(\nu_m - x)J_1(\beta)^2 = 0$. Here we have used the approximation $J_0(\beta)^2 + 2J_1(\beta)^2 \approx 1$, which is valid for the interesting range $\beta \leqslant 1$. However, this shift of locking point has little effect on signal detection because the shift is very small ($<$100 Hz) compared with the cavity linewidth, which is typically a few tens of kilohertz.]

Based on the notation from Fig. 3(e) we can express the field of the cavity-transmitted light in the following form:

$$E = E_0 J_0 \exp[-i(\omega t - \phi_x)] + E_0 J_1 \times \exp\{-i[(\omega + \Delta)t + \phi_m - \phi_x]\} - E_0 J_1 \times \exp\{-i[(\omega - \Delta)t + \phi_m - \phi_x]\}. \quad (6)$$

The heterodyne current in the fast photodiode is proportional to $E \times E^*$. When the laser carrier (the central op-

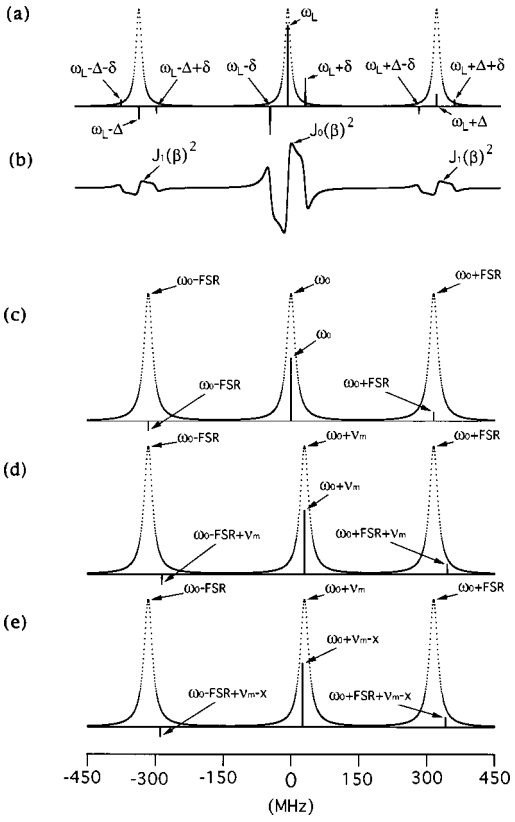

Fig. 3. (a) Optical frequency amplitude spectrum showing cavity resonances and two sets of rf sidebands in the input spectrum. (b) Three contributions to the servo error signal from the output of a balanced mixer demodulated at δ. (c) Transmitted amplitude spectrum, no molecular resonance, laser and sidebands precisely locked onto cavity resonances. (d) Transmitted amplitudes, showing a $+\nu_m$ shift of the central cavity resonance owing to molecular resonance. If only the carrier contributes to the servo, the laser still locks onto the cavity resonance center, which has been shifted. (e) Actually three components contribute to the servo, so the laser lock frequency is shifted relative to cavity resonances by a reduced amount $x = 2\nu_m J_1(\beta)^2$.

tical frequency component) interacts with the saturated molecular absorption, the signal current is derived to be

$$i_s = g4J_0(\beta)J_1(\beta)\sin(\Delta t)\sin(\phi_m), \tag{7}$$

which has a pure dispersion line shape and which is independent of the laser–cavity locking point. Here g is a scaling constant and ϕ_m and ϕ_x are the phase shifts that are due to frequency shift ν_m and locking offset x, respectively. $J_0(\beta)$ and $J_1(\beta)$ are the zeroth- and first-order Bessel functions with index β. An extremely important aspect of this response is that it contains only the odd-symmetric response $\sim\sin(\phi_m)\sin(\Delta t)$, so the line shape and the apparent line-center position are independent of any nonoptimal setting of the rf detection phase. This property will permit extremely precise locking to these resonances, even though the rather high modulation frequency ($\sim$400 MHz) will make stability of the detection phase problematic.

Because the final saturation signal is obtained by dither-lock-in detection, the line shape presented in Eq. (7) will then take the form of a derivative of dispersion, which was studied by Smith based on the original Walquist analysis.[18] Following Smith's notation, the first-harmonic detection gives the following signal:

$$\text{Signal} = 2 - (Y/D), \tag{8}$$

where $Y = (U^2 - 2U)^{1/2}$, $U = I + D$, $D = (I^2 - 4A^2)^{1/2}$, $I = 1 + A^2 + B^2$, $B = H_{1/2}/(2H_\omega)$, and $A = H_\delta/H_\omega$. The FWHM of molecular resonance is $H_{1/2}$, H_ω is the modulation amplitude, and H_δ is the laser-frequency detuning. This basic line shape is often used to fit our experimentally scanned resonance data from the spectrometer, such as in Fig. 9 below.

D. Signal Size and Discrimination Slope

The implicit power-density buildup of the resonator is valuable in producing the high levels of circulating power needed to give appreciable saturation while at the same time requiring the detector to accept only a modest power. The latter point is important because the best possible noise increase with detected power would be the $P^{1/2}$ dependence of shot noise. At higher power intensity, noise of a technical origin will dominate, leading to a P^1 increase of detected noise. So the (resonant) cavity transmission T should be chosen to be a suitable value when the cavity input power is fixed. To get the most efficient input coupling, we pick $T_{\text{in}} = T_{\text{out}} + L_{\text{in}} + L_{\text{out}} + 2\alpha L$ from Eq. (2). Therefore this input coupling gives near-zero reflection and so produces the highest contrast in the cavity-reflected beam. The cavity output and input couplings can be found from Eqs. (1)–(3) and are given by

$$T_{\text{out}} = T/(1 - T)(L_{\text{in}} + L_{\text{out}} + 2\alpha L),$$

$$T_{\text{in}} = T_{\text{out}}/T.$$

The intracavity gas pressure not only affects the molecular resonance linewidth, thereby modifying the saturation intensity that is due to the absorption of αL, as indicated in Eq. (4), but also changes the efficiency of input power coupling into the cavity. Therefore the signal size and its discriminator slope will inevitably vary, depending on the pressure that we use. This is a rich problem to analyze in detail because of the intensity periodicity along the cavity axis. However, a useful modeling of the behavior can be based on an axially averaged field picture[12,19] in which the moving molecules interact with the average standing intracavity field. At resonance, the counterrunning waves in the Fabry–Perot cavity interact with the same molecules, causing the absorption coefficient to be reduced from the off-resonance value of $\alpha_0/(1 + S)^{1/2}$ to $\alpha_0/(1 + 2S)^{1/2}$. Here α_0 is the linear absorption coefficient at the center of the Doppler profile and S is the saturation parameter. The observed nonlinear signal is then proportional to[12]

$$\Delta\alpha = \frac{\alpha_0}{\sqrt{1 + S}} - \frac{\alpha_0}{\sqrt{1 + 2S}}. \tag{9}$$

For calculations we use Eqs. (1)–(4) and the following useful relations: $\Delta n = \Delta\alpha\lambda/4\pi$, $\alpha_0 = \alpha_m P$, and $I_{\text{sat}} = \rho[1 + (\Gamma_p P/\Gamma_T)^2]$, where Δn is the refractive-index change that is due to saturated molecules and α_m is the molecular absorption coefficient per unit length and unit pressure. P is the gas pressure. I_{sat} is the required saturation intensity (in units of watts per square millimeter) for the saturation parameter of 1, and ρ is a power-scaling constant that can be related to the transition dipole moment. It can also be determined by experimental data, as shown in Subsection 4.D below. Coefficient Γ_T is the transit-time broadening, while T_p is the pressure broadening rate. We can now calculate in steps the relative depth of the saturated absorption in the cavity, the cavity frequency shift that is due to the molecular resonance, and the FM signal size and discrimination slope as functions of gas pressure.

Figure 4 is an example of calculation for the $P(11)$ line of the C_2H_2 ($\nu_1 + 3\nu_3$) band at 790 nm. Notice that the optimal pressure for maximum signal slope is slightly less than for maximum signal size.

E. Shot-Noise Limited Sensitivity

The signal size is proportional to the product of carrier and sideband field amplitudes [$\sim J_0(\beta)J_1(\beta)$], whereas the shot noise is determined by the total power on the detector. The S/N can be derived in the following steps:

$$\bar{i}^2_{\text{signal}} = 8\left[\frac{e\eta P_0 J_0(\beta)J_1(\beta)\sin(\phi_m)}{h\nu}\right]^2,$$

$$\bar{i}^2_{\text{noise}} = 2eB\frac{e\eta}{h\nu}P_0,$$

$$(S/N)^2 = \frac{\bar{i}^2_{\text{signal}}}{\bar{i}^2_{\text{noise}}} = \frac{4\eta P_0[J_0(\beta)J_1(\beta)\sin(\phi_m)]^2}{h\nu B}, \tag{10}$$

where h is Planck's constant, B is the detection bandwidth, η is the detector's quantum efficiency, and P_0 is the light power on the detector. [Here we have again used the approximation $J_0(\beta)^2 + 2J_1(\beta)^2 \sim 1$, which is valid for β in the interesting range $\leqslant 1$.]

The minimum detectable molecular phase shift in a shot-noise-limited detection can be found when the signal's peak-to-peak size is twice the standard deviation of noise, i.e., $(S/N)^2 = 4$ in Eq. (10). This intracavity mo-

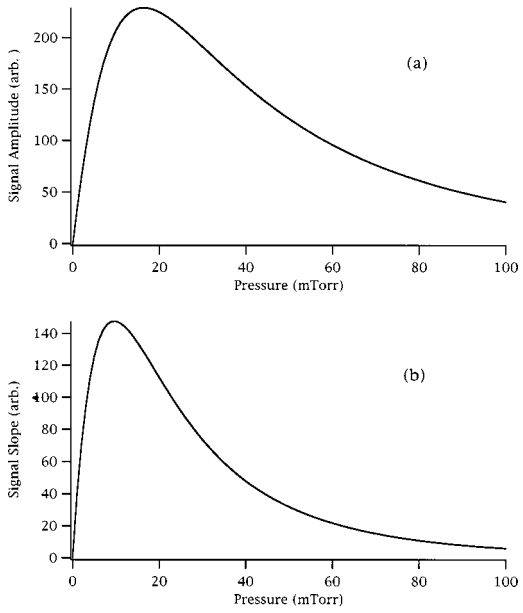

Fig. 4. Calculation of molecular signal size and its discrimination curve slope with respect to intracavity gas pressure. Input optical power is fixed at 14.5 mW. The molecular parameters are for $P(11)$ of the C_2H_2 ($\nu_1 + 3\nu_3$) band at 790 nm. Assumed cavity finesse, 1.7×10^4; input and output coupling coefficients, 48 and 8 ppm, respectively; the total absorption and scatter loss, 310 ppm.

lecular phase leads to a shift of the cavity resonance, expressed in terms of $\tan(\phi_m) = -\nu_m/\nu_{1/2}$, where $\nu_{1/2}$ is the HWHM of the cavity. At the same time, we can also express ν_m as $-\omega_0 \Delta n$. Using the relation $\Delta\alpha = \Delta n \lambda/(4\pi)$, we can derive the detectable integrated absorption at the shot-noise limit:

$$\Delta\alpha L = \frac{\pi}{F}\sqrt{\frac{h\nu B}{\eta P_0}}\,\frac{1}{J_0(\beta)J_1(\beta)}, \tag{11}$$

where F is the finesse of the cavity, λ is the wavelength, and $\Delta\alpha$ is the depth of saturated absorption as indicated in Eq. (9). As an example, when $\lambda = 1064$ nm, $F = 1 \times 10^5$, $P_0 = 4$ mW, $\eta = 0.85$, and $\beta = 0.5$, the following value is obtained from Eq. (11): $\Delta\alpha L = 4 \times 10^{-13}$ (for a 1-s averaging time).

3. EXPERIMENTAL CONFIGURATION

A. Optical and Modulation Consideration

Figure 5 shows the experimental setup for the spectroscopic studies of the C_2H_2 and C_2HD overtone transitions. A frequency stabilized JILA-designed Ti:sapphire laser was used as the light source in the 790-nm region where the ($\nu_1 + 3\nu_3$) band of C_2H_2 is located. For the study of the $P(5)$ line of the C_2HD ($\nu_2 + 3\nu_3$) band at 1064 nm, a commercial diode-pumped solid-state nonplanar ring Nd:YAG laser (NPRO) was used. An acousto-optic modulator (AOM) was placed at the laser output to serve as an intensity stabilizer and as an optical isolator. Two separate EOM's made from $LiTaO_3$ were used to phase modulate the laser beam to impose two sets of FM sidebands. The first, EOM1, used at Δ = FSR, was connected to a high-Q ring inductor to make a rf resonant tank that efficiently couples the rf power into the EOM crystal.[20] The signal source was a stable frequency synthesizer amplified to ~0.5 W. The second, EOM2, was also driven by a rf tank circuit, resonating at 4 MHz. Although our new noise-immune method frees one from needing the extreme accuracy of locking the laser onto the cavity within the shot-noise limit to suppress converted frequency noise, the laser still needs to be locked to the extent that its full energy spectrum is narrowed enough to be usefully coupled into the cavity. For this we use the rf sideband (at $\delta/2\pi = 4$ MHz) locking technique,[21] working with light reflected from the cavity. The reflected beam from the cavity was steered onto a P–I–N photodiode by a quarter-wave plate ($\lambda/4$) and a polarizing beam splitter (PBS). The 4-MHz sidebands lie far outside the cavity linewidth and serve in the usual way as the heterodyne reference fields for the cavity's leakage field. Phase-sensitive demodulation of the 4-MHz photo beat produced an error signal that was used for laser-frequency stabilization, with the amplified and filtered correction signals being fed to the laser cavity piezoelectric transducer (PZT) and to an external frequency stabilizer system[2] through EOM3–AOM2 in Fig. 5. With the fast servo bandwidth offered by the external frequency stabilizer, we have reached a relatively low frequency-noise-density of 0.35 Hz/$\sqrt{\text{Hz}}$, corresponding to a 0.4-Hz laser linewidth relative to the cavity when the Ti:sapphire laser source was being used. The limit at present is fixed only by the choice of 4-MHz modulation frequency, which provides too slow a Nyquist sampling rate for the multimegahertz bandwidth needed when the Ti:sapphire is pumped by a large-frame Ar laser. Inasmuch as the NPRO laser has low inherent frequency noise, the servo gain that was attainable without use of EOM3 was sufficient to provide a low frequency-noise density of 20 mHz/$\sqrt{\text{Hz}}$, corresponding to a 1.3-mHz (Ref. 22) laser linewidth relative to the cavity.

In our experiments, the high-finesse cavity consisted of two mirrors that were spaced by a cylindrical Zerodur. The input coupling mirror was flat and was mounted upon a thin PZT for modulating the cavity length to provide a small audio-frequency dither. The output coupler was a concave mirror, which was mounted upon a PZT for

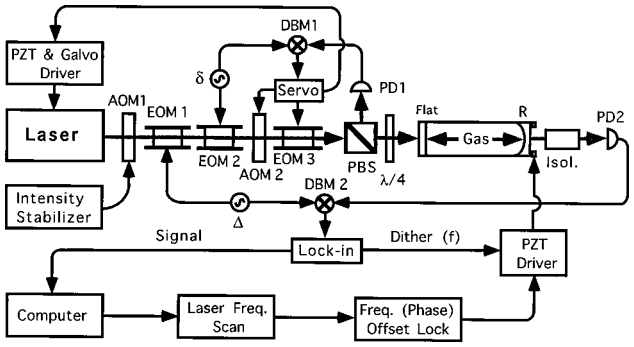

Fig. 5. Experimental configuration for NICE-OHMS. An external stabilizer (AOM–EOM) is employed to widen the frequency servo bandwidth. Sidebands at $\delta/2\pi = 4$ MHz are used for reflection lock to cavity; sidebands at Δ = cavity FSR are used in transmitted light as local oscillators for heterodyne detection of saturated gas absorption inside the cavity. DBM's, double-balanced mixers; PD's, photodiodes; R, concave reflector; other abbreviations defined in text.

tuning the cavity. The empty-cavity finesse was measured by a cavity-field ring-down method: The light intensity reflected from the cavity is monitored by a digital oscilloscope, and the laser frequency is quickly scanned over a cavity resonance. The ring-down decay is produced by the heterodyne beat between the field leaking from the cavity storage and the instantaneous light field reflected at the cavity input coupler. The observed ring-down decay ($e^{-t/\tau}$) is the electric field decay time τ, which corresponds to a cavity full width of $1/(\tau\pi)$. Table 2 lists differences in the experimental setups and the cavities for the studies of C_2H_2 and C_2HD. The aluminum vacuum shell about the cavity, evacuated by a small turbo pump, gave a background pressure of a few times 10^{-5} Torr. The cavity-transmitted beam was steered onto a fast photodetector to detect the rf beat signal at modulation frequency of Δ = FSR when the laser wavelength was tuned onto the molecular resonances. The amplified rf signal was demodulated by a double-balanced mixer. To suppress the noise and dc offsets caused by cavity vibrations and technical defects of EOM 1, we dithered the cavity length (and hence the tightly locked laser frequency) at f = 523 Hz, a local minimum in the observed noise spectrum from the rf balanced mixer. The rf demodulated signal, with a dispersion line shape, was then further processed by an audio lock-in referenced to the 523-Hz dither. We therefore recovered an even-symmetric signal that approximated the derivative of the dispersion line shape.[18] With the use of second-harmonic lock-in detection we could obtain an antisymmetric discrimination signal suitable for locking the laser–cavity system onto the molecular lines.

To enable us to study the line shape of the molecular resonance precisely, our experimental setup at 1064 nm has a laser frequency-offset-lock system referred to another stable laser, and the whole system is controlled by a computer, as shown in Fig. 6. One of NPRO lasers was frequency doubled and locked onto the I_2 transition $R(56)$ 32–0, component a_{10},[3,23] by the modulation transfer technique. Because the digital divider has a speed limitation, the beat frequency was reduced from 5.25 to 3.2 GHz by a mixer and an additional synthesizer and then divided by 64. The phase detector was operated at 45 MHz, and its reference source (at 45 MHz) was frequency modulated by the reference output of the audio lock-in at 523 Hz. Therefore the laser/cavity servo error signal had a feed-forward modulation at 523 Hz to approximate the cavity dither at the same frequency. (Such feed forward reduced the stress on the laser locking loop and is especially helpful as one increases the finesse.) A lock-in amplifier (SR 830 DSP) can recover the fundamental or a harmonic component of the signal. After a small smoothing, its output was recorded by the computer that controlled the frequency of synthesizer 1 to perform precise scanning of the laser frequency. As the frequency scanning was precisely related to an I_2 resonance, the molecular S/N could be improved by averaging of several scans. This process was helpful in the study of optical selection of slow molecules, as we discuss in Subsection 5.B below.

B. Active Lock to Make Δ = FSR

As the length of the high-finesse cavity is changed for laser tuning over a wide range, the cavity's FSR changes.

Table 2. Differences in Experimental Realization of the C_2H_2 and C_2HD Spectrometers

	Absorber (Wavelength)	
Operating Component	HCCD (1064 nm)	HCCH (790 nm)
Laser	Diode-pumped Nd:YAG	Ar^+ pumped Ti:sapphire
EOM3	No	Yes
Output isolation AOM	Yes	No
VCO-FSR lock	Yes	No
Laser–Cavity relative linewidth	1.3 mHz	0.4 Hz
FSR	318.334 MHz	421.196 MHz
Finesse	100,000	17,000
Transmission efficiency	19%	1%
Mode size (w_0)	0.41 mm	0.27 mm

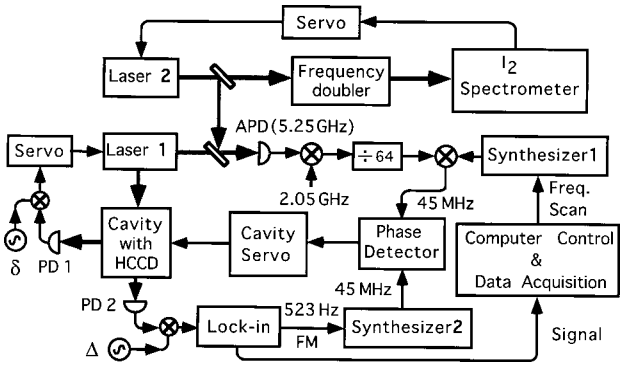

Fig. 6. Precision scanning NPRO–HCCD spectrometer, referenced to an I_2-stabilized NPRO. rf offset between the two laser systems is implemented by a phase-locked loop. PD's, photodiodes; APD, avalanche photodiode.

To reduce increased noise associated with the mismatch between modulation frequency Δ and the changing cavity FSR, frequency Δ must track the cavity length. With a suitable programmable synthesizer for frequency Δ, this could be done under software control. In our experiments, Δ was generated by a low-phase-noise voltage-controlled crystal oscillator (VCXO) with the sideband-dithering technique shown in Fig. 7(a). The VCXO frequency was shifted by synthesizer f_2 to match $f_1 + f_2 = \Delta$ to the FSR. When the modulation frequency Δ is dithered at frequency Ω (by modulation of f_2), the frequency components of the laser beam are as shown in Fig. 7(b) and can be described by the following equation:

$$\begin{aligned}\exp\{i[\omega t + \beta\sin(\Delta t + M\sin\Omega t)]\} &= \exp(i\omega t)\{-J_1(\beta)J_1(M)\exp[i(-\Delta-\Omega)t] \\ &- J_1(\beta)J_0(M)\exp(-i\Delta t) \\ &+ J_1(\beta)J_1(M)\exp[i(-\Delta+\Omega)t)] \\ &+ J_0(\beta) - J_1(\beta)J_1(M)\exp[i(\Delta-\Omega)t] \\ &+ J_1(\beta)J_0(M)\exp(i\Delta t) \\ &+ J_1(\beta)J_1(M)\exp[i(\Delta+\Omega)t]\},\end{aligned} \tag{12}$$

where M is the frequency dither amplitude/Ω.

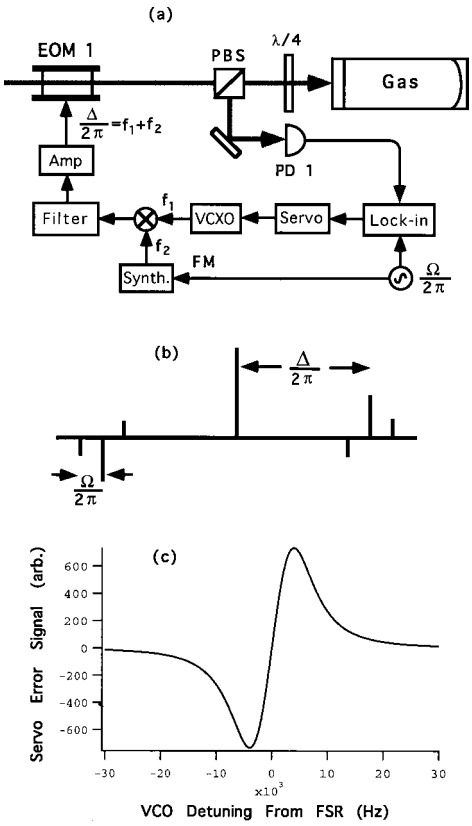

Fig. 7. (a) Experimental scheme for tracking sideband Δ produced by EOM1 to the cavity FSR. The frequency of the low-noise VCXO needs to be shifted by synthesizer f_2 to make $f_1 + f_2 = \Delta$ match the FSR. (b) Optical spectrum of the input beam. (c) Resultant servo error signal after phase-sensitive detection at Ω. PD1, photodiode, PBS, polarizing beam splitter; other abbreviations defined in text.

The cavity-reflected beam is steered onto photodiode PD 1 and demodulated by a lock-in amplifier at frequency Ω. The demodulated signal can be written as follows[24]:

$$\begin{aligned} I_r = {} & J_1(\beta)^2 J_0(M) J_1(M) \mathrm{Re}[+E_r^*(\omega + \Delta) \\ & \times E_r(\omega + \Delta + \Omega) - E_r^*(\omega - \Delta) \\ & \times E_r(\omega - \Delta + \Omega) - E_r(\omega + \Delta) \\ & \times E_r^*(\omega + \Delta - \Omega) + E_r(\omega - \Delta) \\ & \times E_r^*(\omega - \Delta - \Omega)], \end{aligned} \tag{13}$$

where $E_r(\omega) = E_{\mathrm{in}}\sqrt{R}\,\{[1 - \exp(-i2\pi\omega/\mathrm{FSR})\exp(-\alpha L)]\}/[1 - R\exp(-i2\pi\omega/\mathrm{FSR})\exp(-\alpha L)]$ is the field reflected by the optical cavity, $\omega/(2\pi)$ is the frequency of light, R is the reflectivity of the cavity mirrors, and αL is the single-pass absorption.

Because $E_r(\omega \pm \mathrm{FSR}) = E_r(\omega)$, the demodulated signal has a null when $\Delta = \mathrm{FSR}$ [see Eq. (13)]. This means that the servo error signal is independent of the laser detuning as well as of the locking jitter. When the carrier is locked onto a resonant mode of the cavity, the first-harmonic-demodulated signal can be written in the following form:

$$\begin{aligned} I_r = {} & J_1(\beta)^2 J_0(M) J_1(M) \mathrm{Re}[+E_r^*(\Delta) \\ & \times E_r(\Delta + \Omega) - E_r^*(-\Delta) \\ & \times E_r(-\Delta + \Omega) - E_r(\Delta) \\ & \times E_r^*(\Delta - \Omega) + E_r(-\Delta) E_r^*(-\Delta - \Omega)]. \end{aligned} \tag{14}$$

Figure 7(c) shows the antisymmetric signal versus frequency detuning of Δ relative to FSR. This signal was used as the error input for the VCXO servo loop to keep the modulation frequency at $\Delta = \mathrm{FSR}$. Therefore the experimental setup maintained the noise-immune performance, even when the optical frequency was scanned. Furthermore, we could precisely measure the change of cavity FSR by counting the VCXO frequency. We describe the measurements of linear absorption by the VCXO-FSR locking technique in Section 4 below.

C. Experimental Conditions

During the experiments, the cavity was filled with C_2H_2 or C_2HD gas with its pressure ranging from 2 to 100 mTorr (0.28–14 Pa) or 2–60 mTorr (0.28–8.4 Pa), respectively. The optical input power was kept at 15 mW for C_2H_2 and 75 mW for C_2HD measurements. The synthesized C_2HD gas had ~55% purity (HCCD+HCCH) determined by a residual-gas analyzer and 81%/19% of HCCD/HCCH measured by integration of the ^1H resonance in a NMR spectrum. The purity of the C_2H_2 gas was stated to be 99.5%. We further purified the gas by freezing the acetylene with liquid nitrogen and pumping out remaining volatile materials.

4. EXPERIMENTAL RESULTS

A. Line-Shape Fitting and Triplet Spectra

The wide tuning ability of the JILA-designed Ti:sapphire laser was welcome, although for the current studies we scanned its frequency over ranges of only 500 MHz near the $P(11)$ line of the C_2H_2 $(\nu_1 + 3\nu_3)$ band at 790.7 nm. The expected FM triplet spectrum is shown in Fig. 8. These signals were obtained by the first-harmonic detection of the rf mixer's baseband output with the lock-in amplifier referenced to the cavity dither frequency of 523 Hz. The central peak is the molecular saturated dispersion signal associated with the carrier. The two side peaks arise from the contributions of those molecules that interact with both the carrier and one of the sidebands. Both dispersive and absorptive signals are potentially observable for these outer resonances. Notice the flat baseline, a property that is important in frequency standards applications.

To study the signal line shape in detail we used the 1.06-nm frequency-offset-lock system shown in Fig. 6 to scan the NPRO laser frequency and record the signal precisely. Figure 9 shows a typical scan of the C_2HD overtone resonance of the $P(5)$ line in the $(\nu_2 + 3\nu_3)$ band at 1064 nm. The theoretical model of line shape is based on Wahlquist's modulation-broadening formalism for dispersion signals, as described in Eq. (8). The fit residual is shown with 10× magnification.

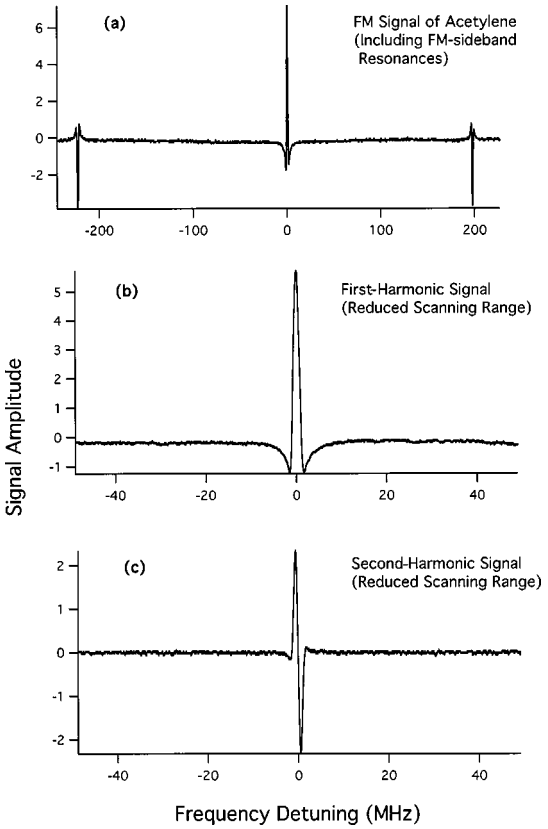

Fig. 8. (a) Triplet spectrum of FM spectroscopy for the $P(11)$ line of the C_2H_2 ($\nu_1 + 3\nu_3$) band at 790.7 nm with the NICE-OHMS setup and dither lock-in detection of the first-harmonic signal. Free spectral range, 422 MHz. Distortion of the frequency axis was produced by PZT nonlinearity in these early data: resonances really occur at ±211 MHz. (b) Reduced laser frequency scanning range. (c) Second-harmonic detection signal with the same scanning range as for (b).

B. Noise-Immune Aspect

In Fig. 10 we illustrate the immunity of our new technique to the laser's residual FM noise. We compared two absorption spectrum cases, one with the normal and one with reduced AOM servo gain in the NPRO system at 1064 nm. The corresponding laser/cavity relative frequency noise levels were ~1.3 mHz and ~10 Hz. We recorded the signals from both the 318-MHz NICE-OHMS channel and the cavity transmission dc channel with the same photodiode. The results show that the new FM technique is insensitive to the locking jitter, whereas, as shown in Fig. 10, the S/N was severely compromised in the other channel. In the same way, we turned the fast external EOM3 frequency stabilizer on and off in the Ti:sapphire laser system at 790.7 nm and obtained results similar to those for the NPRO system. These measurements clearly show the advantage of the frequency noise-immune aspect of the NICE-OHMS method.

C. Absorption Sensitivity Achieved in C_2HD

To illustrate the sensitivity that we achieved with our recent experimental setup, we compare the NICE-OHMS signal with the saturated absorption signal obtained directly in the cavity-transmitted light. For the latter case, which serves to calibrate the absolute absorption, we use a lock-in amplifier to measure the depth of saturated molecular absorption. The actual absorption was obtained with Wahlquist's modulation-broadening formalism for a Lorentz absorption signal.[18] Because we used low gas pressure, the absorption was very small, typically a few percent of 1 part in 10^6 (ppm), and was much below the total loss of the cavity (~60 ppm). Thus we can calculate the absolute absorption of a single pass inside the cavity, based on the finesse of the empty cavity and the change in the transmitted light power measured with a photodiode. Figure 11 shows a S/N (normalized for a 1-s time constant) of 7670 obtained in the C_2HD experiment at 1064 nm. With the saturated absorption signal measured to be 4×10^{-3} ppm, we therefore achieved a noise-equivalent sensitivity of $\sim 5 \times 10^{-13}$ with a 1-s averaging time. The calculated shot-noise-limited saturated absorption signal given by Eq. (11) is 4×10^{-13}, with a modulation index of 0.5 for the 318.335-MHz FM sideband and 4 mW of light power on the photodiode. It is evident from Fig. 11 that the dc detection method has very good sensitivity but has not reached the shot-noise limitation because of the presence of the frequency jitter and other technical noise. In contrast, the sensitivity of NICE-OHMS is only 30% above the shot-noise limitation.

D. Linewidth, Signal Size, and Slope versus Pressure

We performed an extensive study of the pressure-broadening effect on a number of lines in the ($\nu_1 + 3\nu_3$)

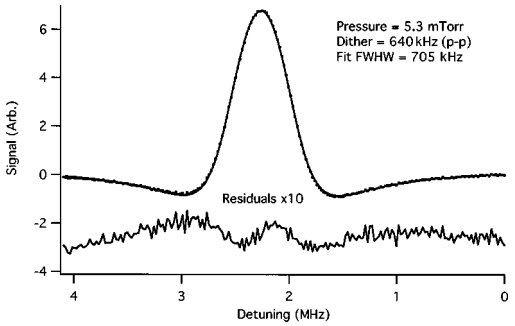

Fig. 9. Frequency scan of C_2HD overtone transitions for the $\nu_2 + 3\nu_3$ band at 1064 nm and overlaid theoretical fit based on the explanation in Ref. 18.

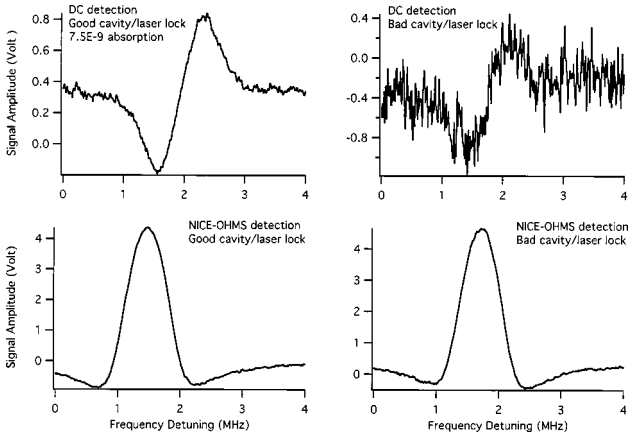

Fig. 10. Comparison of dc and NICE-OHMS detected molecular resonances under the two experimental conditions of tight and loose laser–cavity locks. The apparent line-center shift between top and bottom traces is an artifact of the data processing.

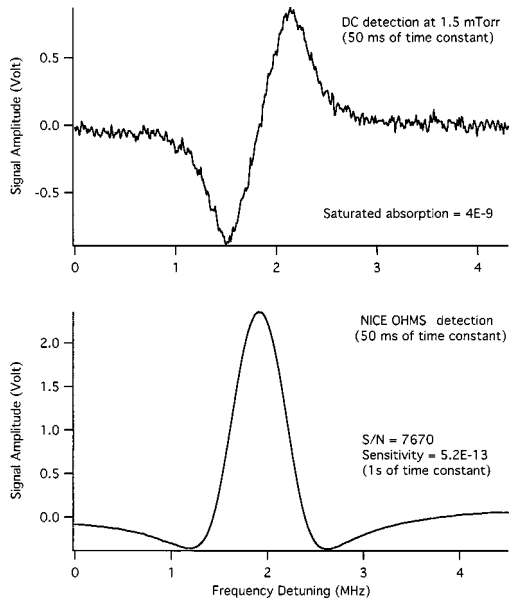

Fig. 11. Estimation of noise-equivalent sensitivity based on the S/N obtained by the NICE-OHMS technique and the saturated absorption level measured by dc detection.

band of C_2H_2 and on the $P(5)$ line in the $(\nu_2 + 3\nu_3)$ band of C_2HD. The C_2H_2 gas pressure was varied from 2 to 100 mTorr (0.28–14 Pa). The acetylene was purified in two steps. First, the container of C_2H_2 was immersed in liquid N_2 for C_2H_2 condensation, and the volatile materials were pumped off. After warming, the C_2H_2 was then further purified by a dry-ice trap on its way to the cavity. We used an MKS Baratron pressuremeter to measure the sample pressure. The C_2HD gas pressure was varied from 2 to 60 mTorr (0.28–8.4 Pa). The light power incident onto the cavity was kept at 14.5 mW for C_2H_2 measurements and at 75 mW for C_2HD experiments. We obtained linewidth by fitting the signal shape with Eq. (8). In the low-pressure case of 2–3 mTorr, we measured the linewidth of the resonance versus the incident light power onto the cavity and thereby obtained the saturation intensity for both molecules. Knowing the saturation at each pressure, we were then able to find the power-broadening contribution to the linewidth and make the corresponding correction. After removing the saturation broadening, we obtained the pressure-broadening coefficients 29.8(0.1) MHz/Torr for the $P(11)$ line of the C_2H_2 $(\nu_1 + 3\nu_3)$ band at 790.7 nm and 34.7 (0.8) MHz/Torr for the $P(5)$ line of C_2HD $(\nu_2 + 3\nu_3)$ band at 1064 nm. In addition, the pressure broadening for $P(1)$, $P(5)$, $P(17)$, and $R(5)$ lines of C_2H_2 in the same band were measured and compared with the $P(11)$ line. Within the measurement accuracy, no differences were evident as a function of the rotational quantum number J. These measurements are shown in Fig. 12. As a result of these measurements, the saturation intensity can be written as follows:

$$I_{\mathrm{sat}} = 1.2 \times 10^3(\Gamma_t/2\pi + 29.8 \times P)^2\ \mathrm{W/mm^2} \quad (\text{for } C_2H_2 \text{ at } 790\,\mathrm{nm}), \quad (15)$$

$$I_{\mathrm{sat}} = 6.1 \times 10^3(\Gamma_t/2\pi + 34.7 \times P)^2\ \mathrm{W/mm^2} \quad (\text{for } C_2HD \text{ at } 1064\,\mathrm{nm}), \quad (16)$$

where $\Gamma_t/2\pi$ is the FWHM (in megahertz) associated with transit time alone, P is the pressure in Torr, and the pressure-broadening rate Γ_p is quoted in MHz/Torr.

Using Eqs. (15)–(16), along with parameters of the experimental setup and the measured absorption coefficients of the gas, we calculated the pressure for maximum signal size and slope. Figure 13 shows the experimental signal slope (signal amplitude/linewidth) versus pressure (filled circles), along with the fitting curves based on the calculation method presented in Section 2. This slope is used as the discriminator for locking, so the maximum slope results in the best locking precision.

E. Linear Absorption Measured by VCO–FSR Locking

For some purposes it is helpful to know the absolute value of the absorption that we are measuring. In this connection the voltage-controlled-oscillator– (VCO–)FSR locking technique introduced in Subsection 3.B is ideal: The absorption is mapped into a frequency shift, which is read by a frequency counter. This method also gives ready access to measurement of the linear absorption of a Doppler-broadened resonance, and here we discuss such an experiment.

Gas absorption implies an associated refractive-index change, and the VCO-FSR-locking servo causes the cavity mode frequency to follow those small variations. The two sidebands at $\omega_L \pm \Delta$ have a frequency shift that is due to the refractive-index change given by the following equation:

$$\Delta n_{\pm_1} = -\frac{\alpha}{\sqrt{\pi}}\frac{1}{\Delta\nu_D}\frac{\lambda}{2\pi}(d \pm \Delta)\exp\left[-\frac{(d \pm \Delta)}{\Delta\nu_D}\right]^2. \quad (17)$$

The frequency shifts can be written as

$$\Delta f_{\pm_1} = -(\nu_0 + d \pm \Delta)\Delta n_{\pm}, \quad (18)$$

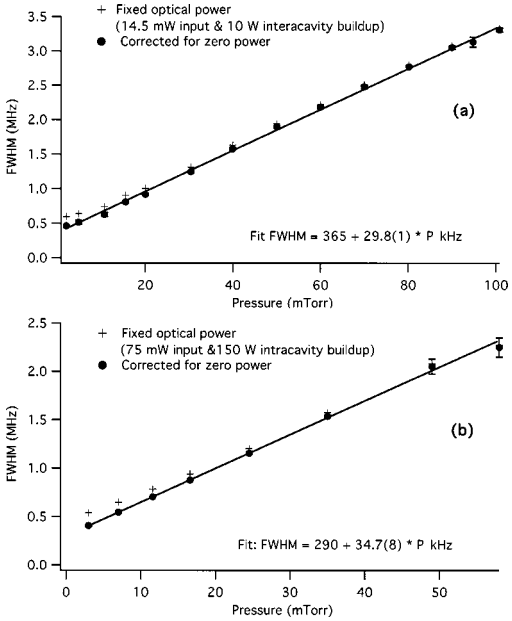

Fig. 12. Pressure-broadening measurement of the overtone transitions. (a) $P(11)$ line in the $(\nu_1 + 3\nu_3)$ overtone band of C_2H_2 at 790 nm. (b) $P(5)$ line in the $(\nu_2 + 3\nu_3)$ band of C_2HD at 1064 nm.

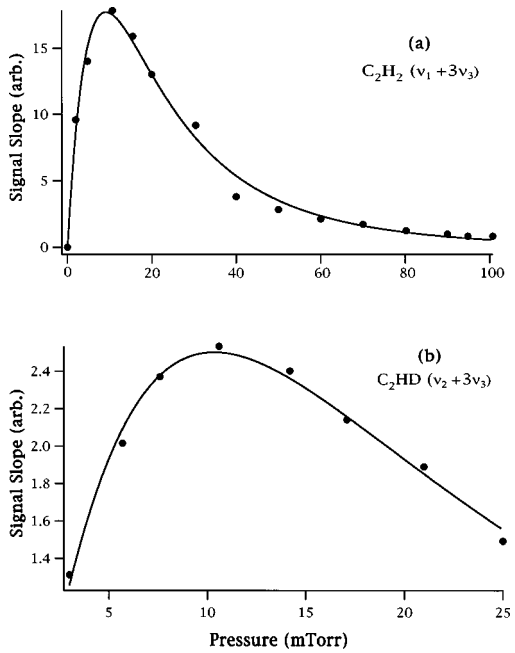

Fig. 13. Molecular signal slope versus gas pressure. Filled circles, experimental data; solid curves, fitted curves. (a) $P(11)$ line, (b) $P(5)$ line.

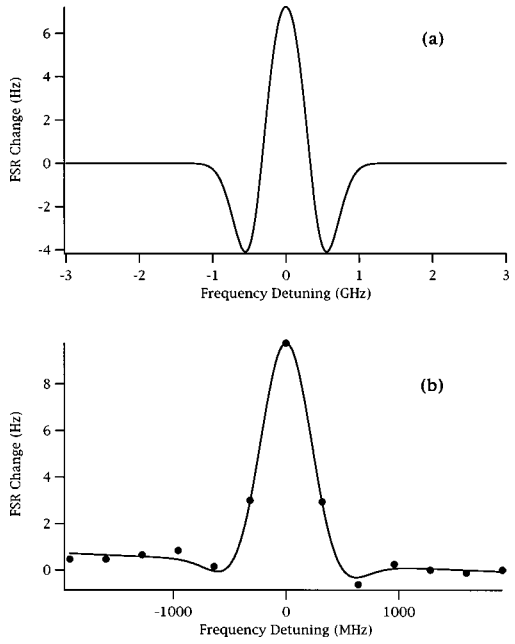

Fig. 14. Signal line shape of intracavity Doppler molecular resonance detected by sideband tracking of the cavity FSR. (a) Theoretical line shape. (b) Experimental data (with integrated time of 1 s and rms noise of 0.1 Hz in each point) and their overlaid fit.

where ν_0 is the center of the molecular absorption line, α is the absorption coefficient at ν_0, Δ is the modulation frequency, d is the detuning of the laser frequency from the line center, and $\Delta\nu_D$ is the HWHM of the Doppler absorption profile.

Inasmuch as the VCO is locked onto the FSR of the cavity, its frequency is changed by

$$\Delta f = (\Delta f_{+1} - \Delta f_{-1})/2. \tag{19}$$

Figure 14(a) shows a calculation based on Eqs. (17)–(19), and the experimental results are shown in Fig. 14(b). We took these data by counting the VCXO frequency while the laser was locked successively onto each adjacent cavity mode, with the length of cavity kept fixed. The C_2HD gas pressure was 10 mTorr, and the optical input power was 2 mW for these experiments. At the present stage of our experiments, we find that the equivalent sensitivity with this method is roughly 200-fold worse than that obtained with NICE-OHMS as in Fig. 11. Other modulation–demodulation strategies appear favorable for reducing this sensitivity penalty.

5. APPLICATION OF NICE-OHMS

A. Stabilization of the Nd:YAG Laser at 1064 nm

We have demonstrated that our new modulation method is a powerful tool to lock the laser frequency onto molecular overtone transitions.[9,10] For operating the device as a molecular frequency reference, it is important to use operating parameters that maximize the signal slope, because the high-gain servo will convert the observed intensity noise into frequency fluctuations according to the inverse of this quantity. In general, the servo error signal is determined by many parameters of the experimental setup, such as incident light power onto the cavity, cavity finesse and efficiency, and gas pressure. Figure 13 shows the optimum choice to be near a pressure of 10 mTorr for the C_2HD spectrometer at 1064 nm. In this range the collision broadening is nearly the same as the transit-time broadening, whereas the saturation parameter is ~0.2, which causes relatively little power broadening. (If even more intracavity power were available, these optimum values would increase somewhat.) Figure 15(a) shows the frequency-discriminator signal used for laser stabilization, which was obtained by second-harmonic detection (relative to the 523-Hz dither frequency) of the spectrometer's basic dispersion resonance line shape. The cavity finesse was 31,900. As shown in the experimental setup of Fig. 15(b), to test the stability of this proposed C_2HD overtone frequency reference we compared the C_2HD-stabilized laser with another NPRO stabilized on an I_2 resonance.[3] The counted beat frequency is plotted in Fig. 16, in which the difference of two optical frequencies shows a drift of ~1.5 Hz/h. In even longer runs a slowly increasing noise in the beat was due to the less-than-perfect cavity vacuum system, now improved, which gradually contaminated the intracavity gas. The frequency reference for the measurement, NPRO I, was frequency doubled to 532 nm and locked to component a_{10} of the I_2 $R(56)$ 32–0 transition.[3] With the mean value of the beat frequency between the two lasers measured as 5252.2261 ± 0.0026 MHz and using the a_{10} frequency of 563 260 223.471 MHz ± 40 kHz,[3] we determined the absolute frequency of the $P(5)$ line in the ($\nu_2 + 3\nu_3$) band of $^{12}C_2HD$ to be 281 635 363.962 MHz ± 20.2 kHz. The 20-kHz uncertainty is due mainly to limited knowledge of the absolute frequency of the NPRO I_2 spectrometer, our secondary standard. With 1-s averaging time we obtained a frequency noise of ±60 Hz on the IR beat, in good agreement with the S/N available at 1064 nm. The corresponding Allan deviation is $\sigma_y = 2.0 \times 10^{-13}/\sqrt{\tau}$ (at 1 s of integration time) and im-

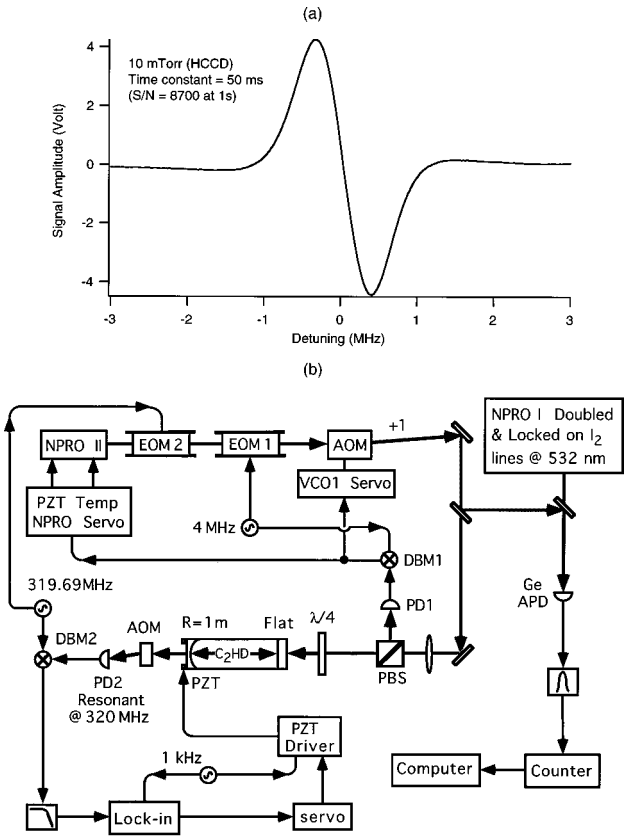

Fig. 15. (a) NICE OHMS signal used for locking the NPRO–cavity system onto the C_2HD resonance. (b) Experimental setup for heterodyne beat between the two MISER systems, one locked on the C_2HD resonance and the other frequency doubled and locked onto an I_2 reference at 532 nm. Abbreviations defined in text and previous figure captions.

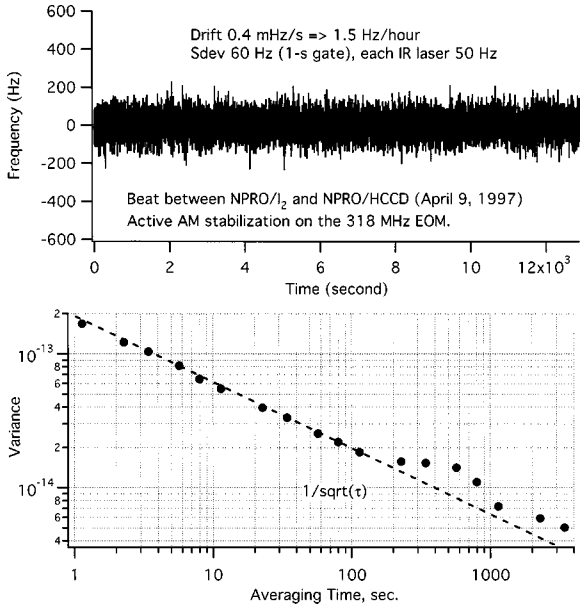

Fig. 16. Time record of the beat frequency between the two NPRO's. The frequency offset of 5252.2254 ± 0.0026 MHz in the beat is suppressed. The Allan variance is calculated from these data.

proves to $<1 \times 10^{-14}$ at a longer integration time (>800 s), a promising indicator for an ultrastable frequency reference. The visible noise bump near ~600 s on the Allan deviation diagram was associated with the lab room-temperature cycling period. (At 532 nm the NPRO I_2 reference system has a 20-Hz rms, 4×10^{-14} frequency noise at 1 s, as tested with a second, I_2-stabilized, NPRO system).

B. Optical Selection of Slow Molecules

Optical selection of slow molecules has been investigated in detail[25] since 1991, although the basic phenomenon and the resultant line shape were studied theoretically much earlier.[11] This method offers the narrowing of linewidth associated with transit-time broadening. It works by operating the spectrometer in a low-power, low-pressure regime within which only the slower molecules make an appreciable contribution to the saturated absorption signal. At starkly reduced power and at lower gas pressure, the saturated absorption signal on these molecular overtone transitions is extremely weak and would no longer be detectable by a normal spectrometer. Owing to its ultrahigh sensitivity, our NICE-OHMS technique allowed us to investigate such weak Doppler-free signals.

Because the natural lifetime is ~300 times longer than our current transit time, we do have the possibility to narrow the linewidth of the overtone transition by optically selecting slow molecules. The experiment was carried out at 1064 nm with C_2HD. The cavity input power was reduced from our maximum available power of 75 mW to 1 mW, where the low Rabi frequency leads to appreciable saturation only for the slowest molecules. As we mentioned above, low gas pressure is required. So the sample gas with a pressure of less than 2 mTorr was filled into the high-finesse cavity where the mean free path of molecules was ~30 times longer than the transverse field dimension, thereby creating a so-called pure transit-time regime. When the light power and the gas pressure inside the cavity are low enough, the saturation becomes inhomogeneous, with molecules from different transverse velocity groups contributing different intensities and widths. Slow molecules that spend their whole lifetimes inside the field will have a constant and velocity-independent saturation parameter, controlled primarily by the collisional broadening. On the other hand, faster-moving molecules have a shorter interaction time with the light field and will thus see a reduced saturation and contribute mostly to the wings of the resonance. Figure 17 shows a resonance with an observed linewidth of ~20 kHz, without correction for the modulation broadening by a 30-kHz peak-to-peak (p-p) dither of the cavity. This linewidth is 13 times narrower than that set by the room-temperature transit time and is limited mainly by the relatively high pressure of 1.8 mTorr.

6. SUMMARY AND FUTURE OUTLOOK

We have demonstrated that our new sensitive detection method can use a high-finesse cavity to improve the signal contrast without the usual frequency-to-amplitude noise conversion by the cavity. Therefore the sensitivity

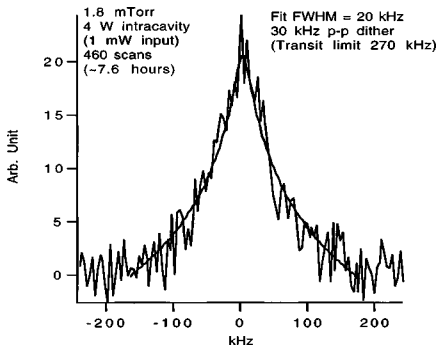

Fig. 17. Observation of slow molecules in our buildup cavity with low optical power and pressure (1-mW input, 1.8 mTorr). The linewidth is narrowed 13-fold below the transit limit.

of this spectrometer can be enhanced directly by the factor of cavity finesse and approaches the ultimate sensitivity limit set only by shot noise. With our 1064-nm laser spectrometer, the sensitivity recently reached the $\sim 5 \times 10^{-13}$ level of integrated absorption, normalized to a 1-s time constant, which is a factor of ~1.4 away from the ideal shot-noise limit. Using our new method of NICE-OHMS, we have provided a valuable optical frequency reference at 1064 nm. After 800 s of integration, an Allan deviation of 1×10^{-14} was recorded. We optically selected slow molecules by reducing light intensity and gas pressure, and a 13-fold reduction in linewidth was observed. Considering that even the $5\nu_3$ band of C_2H_2 at 641 nm has a transition dipole moment that is similar to that of the $(\nu_2 + 3\nu_3)$ band of $^{12}C_2HD$ at 1064 nm, we indeed have a rich collection of overtone resonances that we can study: Clearly it is possible to provide comblike highly stable optical frequency references from the near IR region into the visible by locking the laser frequency onto molecular overtone transitions. In fact, in our current exploration of the 790-nm system we have already mapped out at least ten rotational lines in the $(\nu_1 + 3\nu_3)$ band of C_2H_2 and found improved molecular constants.[26] In future experiments these lines will be linked by their optical frequencies.

We have started building another NPRO C_2HD system with a cavity finesse exceeding 100,000. The intracavity mode size will be increased three-fold by a 52-m radius-of-curvature concave mirror, reducing the transit-time limit to ~90 kHz. With the increased detection sensitivity and narrower linewidth, we should be able to improve our short-term frequency noise to ~30 Hz (1×10^{-13}) at 1-s averaging. A linewidth of a few tens of kilohertz with the improved S/N offered by slow molecules will help to maintain a high level of long-term stability and reproducibility. Meanwhile, ultrahigh-resolution spectroscopy of these and other molecular overtone transitions will also be conducted with the aim of resolving hyperfine structures and recoil splittings, thus opening a qualitatively new regime of molecular overtone research.

Considering the small value of the absorption coefficient of this overtone line of C_2HD, we are exploring the possibility of using stronger overtone transitions to further improve the S/N and consequently the frequency stability. These lines do exist, even in the visible, lying within the tuning ranges of diode or Ti:sapphire lasers. For example, the absorption coefficients in the $(\nu_1 + 3\nu_3)$ band of C_2H_2 at 790 nm are ~20 times larger than those that we used in the $(\nu_2 + 3\nu_3)$ band of $^{12}C_2HD$ at 1064 nm. Commercially available diode lasers can emit a >50-mW coherent light beam at 790 nm. It is certainly ambitious but not far-fetched to expect a 1×10^{-14} short-term stability with 1-s averaging time, with a transition ten times stronger than that of C_2HD presented here. Research in this direction is in progress.

Sensitive detections of linear absorption have potential applications in environmental science and in molecular spectroscopy. The VCXO-FSR locking technique is certainly one of the promising methods that can provide precise measurement of weak absorptions. One can foresee an easy integration of a broadly tunable laser with this technique and operation of it under computer supervision to provide spectra of unrivaled sensitivity and accuracy.

ACKNOWLEDGMENTS

The authors are grateful to Bruce Tiemann, who synthesized the HCCD gas sample for our experiment. This research was supported in part by the National Institute of Standards and Technology as part of its program of exploratory research supporting potential future basic standards and in part by the U.S. Office of Naval Research, the U.S. Air Force Office of Scientific Research, and the National Science Foundation.

*Permanent address, Laboratory for Quantum Optics, East China Normal University, Shanghai, China.

†Present address, TRIUMF, Vancouver postal code British Columbia, Canada

‡Present address, Quantum Physics Division, National Institute of Standards and Technology, Boulder, Colorado 80303.

REFERENCES AND NOTES

1. Under shot-noise-limited conditions, the minimum detectable absorption is $\Delta\alpha L = 2[h\nu B/(\eta P_0)]^{1/2}/[J_0(\beta)J_1(\beta)] = 3.2 \times 10^{-7}$, where $P_0 = 0.1$ mW, $B = 1$ Hz, $\beta = 1$, $\lambda = 790.7$ nm, and $\eta = 0.8$.
2. M. Zhu and J. L. Hall, "Stabilization of optical frequency/phase of a laser system: application to a commercial dye laser with an external stabilizer," J. Opt. Soc. Am. B **10**, 802–816 (1993).
3. P. Jungner, S. Swartz, M. Eickhoff, J. Ye, J. L. Hall, and S. Waltman, "Absolute frequency of the molecular iodine transition $R(56)32-0$ near 532 nm," IEEE Trans. Instrum. Meas. **44**, 151–154 (1995); P. Jungner, M. Eickhoff, S. Swartz, J. Ye, J. L. Hall, and S. Waltman, "Stability and absolute frequency of molecular iodine transitions near 532 nm," in *Laser Frequency Stabilization and Noise Reduction*, Y. Shevy, ed., Proc. SPIE **2378**, 22–34 (1995); J. L. Hall, L.-S. Ma, M. Taubman, B. Tiemann, F. L. Hong, O. Pfister, and J. Ye, "Stabilization and frequency measurement of the I_2-stabilized Nd:YAG laser," IEEE Trans. Instrum. Meas. **48**, 583–586 (1999).
4. M. de Labachelerie, K. Nakagawa, and M. Ohtsu, "Ultranarrow $^{13}C_2H_2$ saturated absorption lines at 1.5 μm," Opt. Lett. **19**, 840–842 (1994); M. de Labachelerie, K. Nakagawa, Y. Awaji, and M. Ohtsu, "High-frequency-stability laser at 1.5 μm using Doppler-free molecular lines," Opt. Lett. **20**, 572–574 (1995); K. Nakagawa, M. de Labachele-

rie, Y. Awaji, and M. Kurogi, "Accurate optical frequency atlas of the 1.5-μm bands of acetylene," J. Opt. Soc. Am. B **13**, 2708–2714 (1996).
5. L. S. Ma, P. Dubé, J. Ye, and J. L. Hall, "Saturation spectroscopy of molecular overtones for laser frequency standards in the visible and near-visible domain," in *Quantum Electronics and Laser Science Conference*, Vol. 16 of 1995 OSA Technical Digest Series (Optical Society of America, Washington, D.C., 1995), p. 18.
6. P. Cerez, A. Brillet, C. N. Man-Pichot, and R. Felder, "He–Ne lasers stabilized by saturated absorption in iodine at 612 nm," IEEE Trans Instrum. Meas. **29**, 352–354 (1980).
7. L. S. Ma and J. L. Hall, "Optical heterodyne spectroscopy enhanced by an external optical cavity: toward improved working standards," IEEE J. Quantum Electron. **26**, 2006–2012 (1990).
8. L. S. Ma, J. Ye, P. Dubé, and J. L. Hall, "A new modulation method for sensitive nonlinear spectroscopy—application to molecular overtones as visible frequency references," in *Laser Spectroscopy XII*, M. Inguscio, M. Allegrini, and A. Sasso, eds. (World Scientific, Singapore, 1995), pp. 199–203; J. L. Hall, J. Ye, L.-S. Ma, S. Swartz, P. Jungner, and S. Waltman, "Optical frequency standards—some improvements, some measurements, and some dreams," in *Fifth Symposium on Frequency Standards & Metrology*, J. C. Bergquist, ed. (World Scientific, Singapore, 1995), pp. 267–276.
9. J. Ye, L.-S. Ma, and J. L. Hall, "Sub-Doppler optical frequency reference at 1.064 μm via ultrasensitive cavity-enhanced frequency modulation spectroscopy of C_2HD overtone transition," Opt. Lett. **21**, 1000–1002 (1996).
10. J. Ye, L.-S. Ma, and J. L. Hall, "Ultrastable optical frequency reference at 1.064 μm using C_2HD molecular overtone reference," IEEE Trans Instrum. Meas. **46**, 178–182 (1997).
11. C. J. Bordé, J. L. Hall, C. V. Kunasz, and D. G. Hummer, "Saturated absorption line shape. Calculation of the transit-time broadening by a perturbation approach," Phys. Rev. A **14**, 236–263 (1976).
12. V. S. Letokhev and V. P. Chebotayev, *Nonlinear Laser Spectroscopy* (Springer-Verlag, Berlin, 1977).
13. J. Vander Auwera, D. Hurtmans, M. Carleer, and M. Herman, "The ν_3 fundamental in C_2H_2," J. Mol. Spectrosc. **157**, 337–357 (1993).
14. M. de Labachelerie, K. Nakagawa, and M. Ohtsu, "Ultranarrow $^{13}C_2H_2$ saturated absorption lines at 1.5 μm," Opt. Lett. **19**, 840–842 (1994).
15. M. A. Temsamani, J. V. Auwera, and M. Herman, "The absorption spectrum of C_2HD between 9000 and 13 000 cm^{-1}," Mol. Phys. **79**, 359–371 (1993).
16. F. S. Pavone, F. Marin, M. Inguscio, K. Ernst, and G. Di Lonardo, "Sensitive detection of acetylene absorption in the visible by using a stabilized AlGaAs diode laser," Appl. Opt. **32**, 259–262 (1993).
17. G. T. Scherer, K. K. Lehmann, and W. Klemperer, "The high resolution visible overtone spectrum of acetylene," J. Chem. Phys. **78**, 2817–2832 (1983); K. K. Lehmann, "The absolute intensity of visible overtone bands of acetylene," J. Chem. Phys. **91**, 2759–2760 (1989).
18. R. L. Smith, "Practical solutions of the lock-in detection problem for Lorentz and dispersion resonance signals," J. Opt. Soc. Am. **61**, 1015–1022 (1971); H. Wahlquist, "Modulation broadening of unsaturated Lorentzian lines," J. Chem. Phys. **35**, 1708–1710 (1961).
19. S. Stenholm, *Foundation of Laser Spectroscopy* (Wiley, New York, 1983).
20. J. F. Kelly and A. Gallagher, "Efficient electro-optic modulator for optical pumping of Na beams," Rev. Sci. Instrum. **58**, 563–566 (1987).
21. R. W. P. Drever, J. L. Hall, F. V. Kowalski, J. Hough, G. M. Ford, A. J. Munley, and H. Ward, "Laser phase and frequency stabilization using an optical resonator," Appl. Phys. B **31**, 97–105 (1983).
22. J. Ye, L.-S. Ma, and J. L. Hall, "Ultrasensitive high resolution laser spectroscopy and its application to optical frequency standards," in *Proceedings of the 28th Annual Precise Time and Time Inteval (PTTI) Applications and Planning Meeting*, L. A. Breakiron, ed. (U.S. Naval Observatory, Washington, D.C., 1997), pp. 289–303.
23. M. L. Eickhoff and J. L. Hall, "Optical frequency standard at 532 nm," IEEE Trans Instrum. Meas. **44**, 155–158 (1995).
24. L.-S. Ma, Ph. Courteille, G. Ritter, W. Neuhauser, and R. Blatt, "Precision laser spectrometer with multiple frequency modulation," in *Digest of International Quantum Electronics Conference* (Optical Society of America, Washington, D.C., 1994), p. 61; Ph. Courteille, L.-S. Ma, G. Ritter, W. Neuhauser, and R. Blatt, "Frequency measurement of Te_2 resonances near 467 nm," Appl. Phys. B **59**, 187–193 (1994).
25. S. N. Bagayev, V. P. Chebotayev, A. K. Dmitriyev, A. E. Om, Yu. V. Nekrasov, and B. N. Skvortsov, "Second-order Doppler-free spectroscopy," Appl. Phys. B: Photophys. Laser Chem. **52**, 63–66 (1991); Ch. Chardonnet, F. Guernet, G. Charton, and Ch. J. Bordé, "Ultrahigh-resolution saturation spectroscopy using slow molecules in an external cell," Appl. Phys. B **59**, 333–343 (1994).
26. J. Ye, "Ultrasensitive high resolution laser spectroscopy and its application to optical frequency standards," Ph.D. dissertation (University of Colorado at Boulder, Boulder, Colo., 1997).